Journal of Asian Earth Sciences 134 (2017) 72–85

Contents lists available at ScienceDirect

Journal of Asian Earth Sciences

journal homepage: www.elsevier.com/locate/jseaes

Full length Article

Melt inclusions in the olivine from the Nantianwan intrusion: Implications for the parental magma of Ni-Cu-(PGE) sulfide-bearing mafic-ultramafic intrusions of the ~260 Ma Emeishan large igneous province (SW China)

Le Zhang [a,b], Zhong-Yuan Ren [a,*], Christina Yan Wang [c]

[a] State Key Laboratory of Isotope Geochemistry, Guangzhou Institute of Geochemistry, Chinese Academy of Sciences, Guangzhou 510640, China
[b] University of Chinese Academy of Sciences (UCAS), Beijing 100049, China
[c] Key Laboratory of Mineralogy and Metallogeny, Guangzhou Institute of Geochemistry, Chinese Academy of Sciences, Guangzhou 510640, China

ARTICLE INFO

Article history:
Received 26 July 2016
Received in revised form 7 November 2016
Accepted 9 November 2016
Available online 10 November 2016

Keywords:
Melt inclusion
Olivine
Nantianwan
Parental magma
The Emeishan large igneous province

ABSTRACT

Olivine-hosted melt inclusions provide an archive of the parental magma and early magma history that is unavailable from bulk-rock analyses of cumulates. For those olivine-bearing mafic-ultramafic intrusions, a combined in situ analysis of major elements and Pb isotopic compositions for the melt inclusions and host olivine crystals may provide an effective way to understand the nature of the parental magma of the intrusions. In this study, we take the Nantianwan intrusion in the Emeishan large igneous province (SW China) as an example to analyze the melt inclusions and the host olivine. The Nantianwan intrusion is mainly composed of gabbronorite, with minor olivine gabbro. The olivine crystals in the olivine gabbro have Fo contents varying from 81.1 to 89.2 and Ni from 0.05 to 0.30 wt.%. The melt inclusion hosted in the most Mg-rich olivine has 50.9 wt.% SiO_2, 1.0 wt.% TiO_2, 15.1 wt.% MgO and 2.9 wt.% $Na_2O + K_2O$, indicating that the parental magma of the intrusion was of high-Mg basaltic composition. The melt inclusions overall have $^{208}Pb/^{206}Pb$ ratios of 2.0567–2.1032 and $^{207}Pb/^{206}Pb$ of 0.8287–0.8481, similar to the Pb isotopic compositions of the Emeishan flood basalts and consistent with insignificant crustal contamination. Given that the Nantianwan intrusion contains the most Mg-rich olivine among the Ni-Cu-(PGE) sulfide-bearing mafic-ultramafic intrusions in the Emeishan LIP, we infer that the composition of the melt inclusion in the most Mg-rich olivine from the Nantianwan intrusion may represent the least evolved parental magma of the Ni-Cu-(PGE) sulfide-bearing mafic-ultramafic intrusions in the Emeishan LIP. This can be further used to constrain the magma process related to Ni-Cu-(PGE) sulfide mineralization.

1. Introduction

The parental magma composition of mafic-ultramafic intrusion is difficult to be constrained from the bulk composition of the cumulates as the bulk compositions of the cumulates differ considerably from those of their parental magmas. One possible way is to take the chilled margins of an intrusion or contemporaneous sills/dikes to represent the composition of the parental magma of the intrusion (Ford, 1981; Hoover, 1989; Greenwood et al., 1990). However, this method is not available if the chilled margins are absent or have been affected by contamination or phenocryst accumulation (Harmer and Sharpe, 1985). If the intrusion has been built through multiple pulses of magma over time with varying compositions (e.g. the Bushveld Complex, Kruger, 2005), the chilled margin only records the composition of the initial pulse of magma. Alternatively, the compositions of the parental magma can be calculated using the compositions of the earliest crystallized cumulus mineral and mineral/melt partition coefficients (Chai and Naldrett, 1992; Chalokwu et al., 1993; Bernstein et al., 1996; Ren et al., 2004). In both cases, fresh samples are required to avoid significant alteration and metasomatism by fluxing of late-stage fluids and intercumulus melts (Boudreau, 1999). On the other hand, melt inclusions are small melt droplets that were trapped by growing crystals in a magma system and may preserve important information of the parental magma (e.g. Sobolev, 1996; Ren et al., 2005; Kent, 2008; Kamenetsky et al., 2012; Liu et al., 2016). The melt inclusions that are trapped within resistant primocrysts may avoid later weathering, hydrothermal alteration or low-temperature metamorphism (Kent, 2008). The melt inclusions hosted in the pla-

* Corresponding author.
E-mail address: zyren@gig.ac.cn (Z.-Y. Ren).

http://dx.doi.org/10.1016/j.jseaes.2016.11.014
1367-9120/

gioclase and apatite of the Skaergaard intrusion are considered to record an emulsion of immiscible Fe- and Si-rich liquids (Jakobsen et al., 2005, 2011). Chromite-hosted melt inclusions in the Stillwater complex provide evidence for the assimilation of country rock into the primitive magma in the formation of chromitite layer (Spandler et al., 2005). Melt inclusions that are trapped in the early-crystallized minerals such as olivine, may be ideal to be used to acquire the compositional variations of the parental or the least evolved magma from which the intrusion formed (Sobolev, 1996; Sours-Page et al., 1999; Danyushevsky et al., 2000; Kent, 2008). In this way, an evolution history of the parental magma can be established. Therefore, melt inclusion could be an important archive to record the variation of magma compositions of intrusive bodies.

A number of mafic-ultramafic intrusions hosting magmatic Ni-Cu-(PGE) sulfide deposits occur in the Emeishan large igneous province (LIP) (Zhou et al., 2002, 2008; Song et al., 2006, 2008; Tao et al., 2007a, 2007b, 2008, 2010; Wang et al., 2005, 2006, 2011, 2012a). As these intrusions have been intensively altered, fresh rocks and cumulus minerals such as olivine and clinopyroxene were not preserved. Although these intrusions are considered to be related to the low-Ti magma series of the Emeishan LIP (Zhou et al., 2008; Wang et al., 2011), the compositions of the parental magmas of these intrusions are difficult to be determined so that the early history of the magma fractionation is hard to be constrained. Several indirect ways have been tried in previous studies and the results indicate that nature of the parental magmas of these intrusions is probably of high-Mg and basaltic composition (Wang et al., 2005; Tao et al., 2008; Zhu et al., 2011). However, the previous studies failed to determine the exact composition of the parental magmas of these intrusions, making it difficult to establish a direct link between the low-Ti magma series and Ni-Cu-(PGE) sulfide-bearing intrusions in the Emeishan LIP.

In this study, we chose the Nantianwan intrusion in the Emeishan LIP and analyzed the chemical compositions of melt inclusions and their host olivine crystals, and Pb isotopic compositions of the melt inclusions and plagioclase crystals. This intrusion has much fresher samples than other sulfide-bearing intrusions in the Emeishan LIP. What is more, to our best knowledge, the Nantianwan intrusion contains the most Mg-rich olivine among the sulfide-bearing intrusions in the Emeishan LIP (e.g. Wang et al., 2005, 2012a; Tao et al., 2008). The data set analyzed in this study enables us to explore the composition of the parental magma of the Nantianwan intrusion and the fractionation process of the magma. Our work demonstrates that the melt inclusion trapped in the most Mg-rich olivine of a mafic-ultramafic intrusion can be well used to constrain the composition of the parental magma of the intrusion, which is critical to the understanding of early-stage history of magma evolution and the potential mineralization of the intrusion.

2. Geological background

The Emeishan LIP is located in the western part of the Yangtze Block and the eastern margin of the Tibetan Plateau, and extends from SW China into northern Vietnam (Xu et al., 2001; Zhou et al., 2002; Song et al., 2008). The Emeishan LIP is mainly composed of flood basalts, which cover an area of more than 2.5×10^5 km^2 with thickness ranging from several hundred meters in the outer zone up and to 5 km in the inner zone (Chung and Jahn, 1995; Xu et al., 2001). The flood basalts are divided into high-Ti and low-Ti series in terms of TiO_2 content and Ti/Y ratio of the rocks (Xu et al., 2001). Although basalts are the most widely distributed rocks in the Emeishan LIP, a few picrites were found in several locations, such as Lijiang, Binchuan and Dali (e.g. Xu et al., 2001; Zhang et al., 2006; Hanski et al., 2010; Kamenetsky et al., 2012). The most Mg-rich picrite (MgO = 27.5 wt.%) and olivine phenocryst (Fo = 93.5) among the whole Emeishan LIP were found in Dali area (Hanski et al., 2010). Recently, according to the continuous spectrum of the Emeishan picrite, Kamenetsky et al. (2012) further divided the Emeishan flood basalts into low-, intermediate- and high-Ti series.

The Emeishan LIP also contains numerous mafic-ultramafic intrusions. Some of the layered intrusions host giant Fe-Ti oxide deposits, whereas other small mafic-ultramafic intrusions/sills host Ni-Cu-(PGE) sulfide deposits. The layered intrusions are considered to be genetically related to high-Ti series, whereas the small mafic-ultramafic intrusions/sills are related to low-Ti series (e.g., Zhou et al., 2008; Wang et al., 2011).

The Nantianwan mafic intrusion in the western part of the Emeishan LIP hosts Ni-Cu-(PGE) sulfide mineralization (Wang et al., 2012a) (Fig. 1). The intrusion is divided into three parts according to the drilling data (Wang et al., 2012a), including olivine gabbro in the lower part, gabbronorite in the upper part and a transitional zone between them (Fig. 1 a and b).

3. Sampling and petrography

The samples NT-38 and NT-40 were collected from the transitional zone and all other samples were collected from the olivine gabbro part of the Nantianwan intrusion (Fig. 1). Except for the sample NT-12 and NT-22, cumulus olivine crystals in the olivine gabbro remain fairly fresh. They are anhedral and vary in size from 0.1 to 2 mm in diameter. They are enclosed in orthopyroxene, clinopyroxene and plagioclase (Fig. 2a and b). The rims of some olivine crystals are partially altered to serpentine. Melt inclusions are observed in many of these olivine crystals. Most of the melt inclusions are rounded or ellipsoidal in shape, which range in size from 20 to 100 μm along the long axis (Fig. 2c–f). The boundaries between melt inclusions and their olivine hosts are clear. No significant interaction phenomenon can be observed. The melt inclusions are composed of silicates, spinel crystals, intergranular melt and tiny droplets of sulfide melt in local places. Olivines are the dominant phase and they distribute randomly in the whole melt inclusion (Fig. 2d). Minor orthopyroxenes and clinopyroxenes also occur in melt inclusions.

4. Analytical method

4.1. Sample preparation

After crushed into small particles, sample with size between 40 and 60 meshes was selected using sieves. Finally, fresh olivine crystals were selected under binocular microscope. The sample NT-12 and NT-22 underwent much heavier alteration than other samples (Fig. 2a and b). Most of the olivine in NT-12 are heavily broken up and partially altered to serpentine, which makes it difficult for us to find melt inclusions. Fortunately, other samples, e.g. NT-26, are much fresher and endured little serpentinization. Because the Nantianwan melt inclusions are mixtures of crystals and glass, homogenization of these melt inclusions is required. Two ways are usually used for homogenization of melt inclusions. One way is to use a microscope heating stage (e.g., Roedder, 1979; Danyushevsky et al., 2002), whereas the other way is to use a 1-atmosphere redox controlled furnace (e.g., Norman et al., 2002; Ren et al., 2005). However, each approach has its advantage and disadvantage (Danyushevsky et al., 2002). A heating stage provides a direct estimate of the trapping temperature of an inclusion, but it

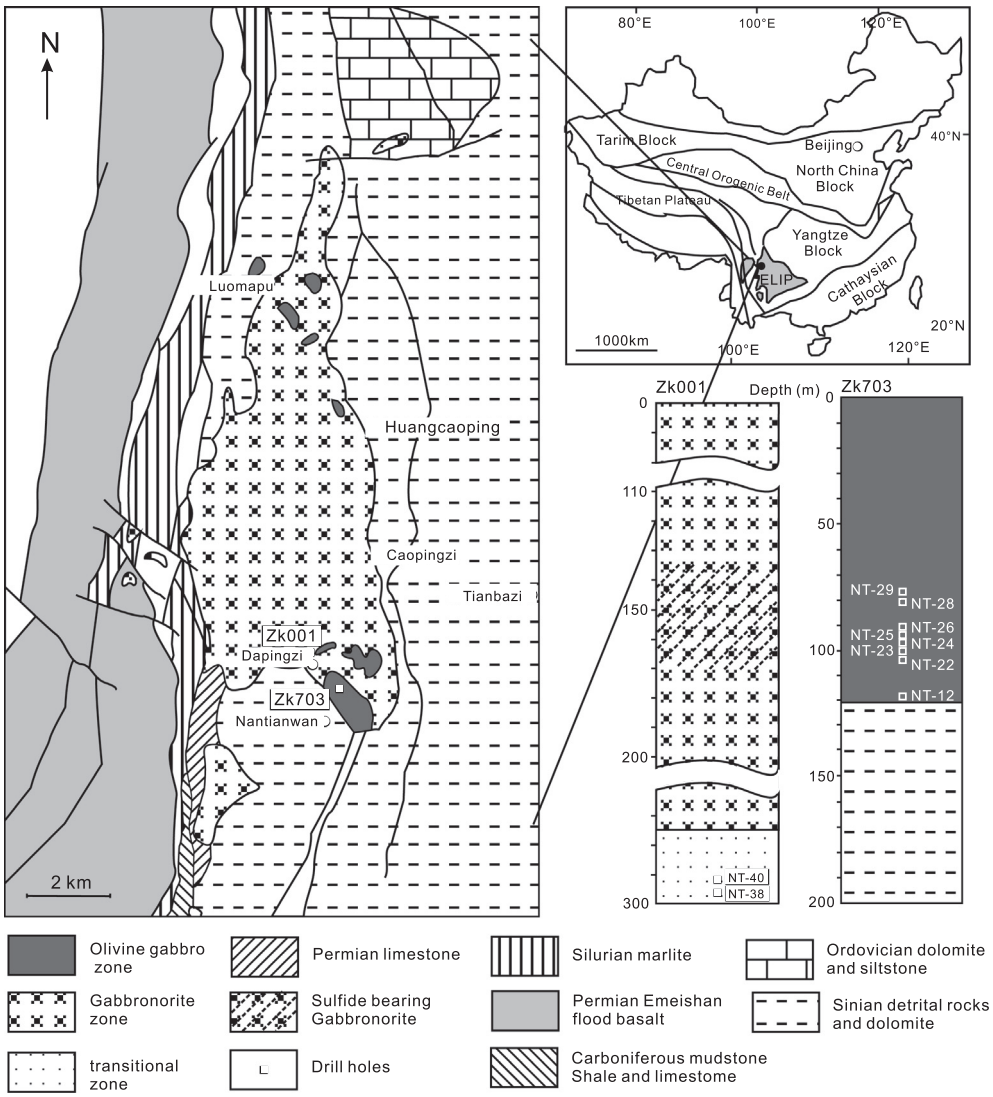

Fig. 1. Geological map of the Nantianwan area, Sichuan Province, SW China (modified after Wang et al., 2012a).

takes long time for sample preparation, and is thus not suitable for vast sample preparation. On the other hand, a gas-mixing furnace is efficient for vast sample preparation, but it cannot directly measure the trapping temperatures so that overheating or underheating of melt inclusion often happens in the process. However, both methods are widely used in the studies of melt inclusions. The melt inclusions from Hawaii basalts show essentially identical results using both methods (Norman et al., 2002).

Homogenization of melt inclusions in this study was processed in a gas-mixing furnace under 1 atm pressure at the controlled quartz-fayalite-magnetite (QFM) buffer through adjusting CO_2 and H_2 gas flow rate following the procedure of Ren et al. (2005). Olivine crystals were heated at a constant temperature (1250 °C) for 10 min and then quickly quenched at room temperature. After homogenization, olivine crystals were mounted in epoxy resin disks and polished until the glassy inclusions were exposed. Melt inclusions with fractures crossing over were discarded to avoid interaction with post-magmatic fluids. All sample preparation was performed at the melt inclusion laboratory in the State Key Laboratory of Isotope Geochemistry, Guangzhou Institute of Geochemistry, Chinese Academy of Sciences (GIGCAS). After homogenization, melt inclusions become compositionally homogeneous glass. Normally a bubble occurs in the homogenized melt inclusion (Fig. 2f).

4.2. Major element compositions of melt inclusion and olivine host

The melt inclusions that are larger than 30 μm in diameter and their olivine hosts were analyzed for major element compositions using JEOL JXA-8100 electron probe microanalysis at the State Key Laboratory of Isotope Geochemistry, GIGCAS, using the procedures of Sobolev et al. (2007) for olivine and Wang and Gaetani (2008) for melt inclusion. Parameters for olivine analyses are set to be 20 kV for accelerating voltage, 300 nA for beam current and 2 μm for spot size. Analyses for melt inclusions were carried out at accelerating voltage of 15 kV, beam current of 20 nA and beam spot of 3 μm. The Na and K of melt inclusions were first measured to avoid their possible loss during analyses. An in-house olivine and a standard glass (JB-2) were measured before and after each analysis session to monitor the instrument drift. The relative standard deviation (2RSD) for the internal olivine standard is 0.2–0.4% for major elements (SiO_2, MgO and FeO), and 1–3% for minor elements (CaO, MnO and NiO), and for JB-2 is <0.5% for most major elements (5, 1 and 7% for MnO, K_2O and P_2O_5, respectively).

4.3. Pb isotopic compositions of melt inclusion and plagioclase

The melt inclusions that are >40 μm in diameter and plagioclase crystals are chosen to be analyzed for Pb isotopic

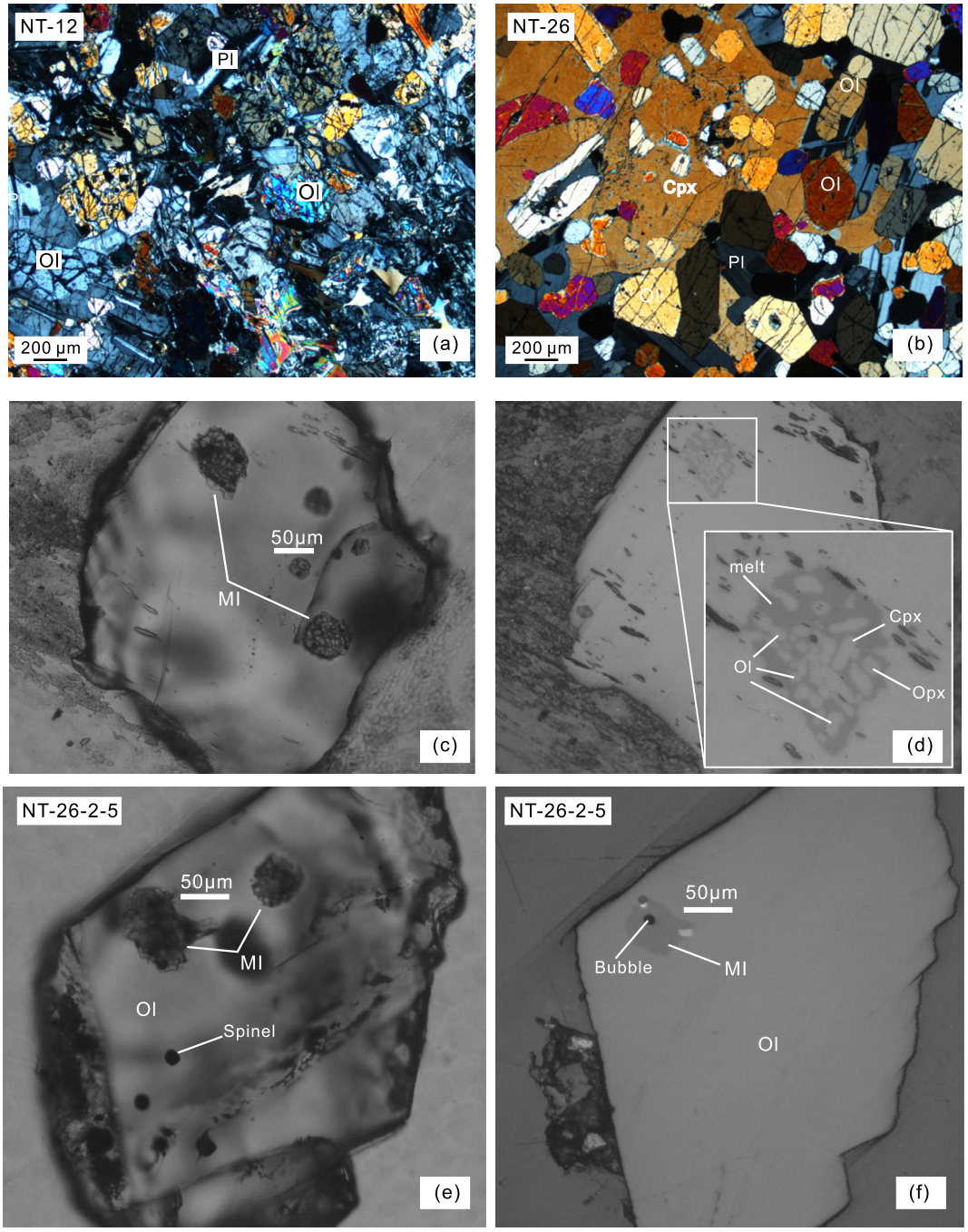

Fig. 2. (a and b) Thin-sections of representative samples of the Nantianwan intrusion. (c) Melt inclusions in olivine crystals from the Nantianwan intrusion (without homogenization; under transmission light). (d) The same sample as in (c) but under reflected light. It shows the unhomogenized melt inclusion consists of silicates (e.g. olivine, orthopyroxene and clinopyroxene) and melt. (e) Melt inclusions after homogenization (under transmission light). (f) The same sample as in (e) but under reflected light. Cpx: clinopyroxene, MI: melt inclusion, Pl: plagioclase, Ol: olivine, Opx: orthopyroxene.

compositions using a Neptune Plus MC-ICP-MS coupled with a 193-nm (ArF) Resonetics RESOlution M-50 laser ablation system in the State Key Laboratory of Isotope Geochemistry, GIGCAS. USGS glass NKT-1G was selected as external standard to correct the mass bias and instrumental drift. The laser parameter was as follow: 45 μm spot size, 3 Hz repetition rate and 80 mJ energy with a 25% energy attenuator. Though the laser spot size is a little larger than some of the melt inclusions, the Pb isotopic compositions will not be affected by ablating little part of their olivine host because (1) Pb is strongly incompatible in olivine and the Pb content in olivine is negligible compared to that in melt inclusions; (2) the olivine host, which crystallized from magma with the same composition as the melt inclusions captured by the olivine host, should have the same Pb isotope compositions as the melt inclusions. Helium (800 ml/min) was the carrier gas and a small flow of nitrogen (2 ml/min) was added into the gas line to enhance the sample signal. Due to the low ^{204}Pb intensity, only the ratios of ^{208}Pb/^{206}Pb and ^{207}Pb/^{206}Pb were used in this study. The detailed procedure of Pb isotope analysis of melt inclusions by LA-MC-ICP-MS was described in Zhang et al. (2014). The average ^{208}Pb/^{206}Pb and ^{207}Pb/^{206}Pb of 18 measurements of USGS glass BHVO-2G are 2.0549 ± 0.0032 and 0.8337 ± 0.0016 (2SD), respectively, which are identical to those recommended by Weis et al. (2005).

5. Analytical results

5.1. Composition of olivine

A total of 53 olivine crystals were analyzed and they have Fo contents varying from 81.1 to 89.2 (Table 1 and Fig. 3). The olivine crystals have 0.12–0.26 wt.% MnO and 0.05–0.30 wt.% NiO, and there are negative correlations of Fo with MnO and NiO (Fig. 3a and b). The CaO contents of the olivine vary from 0.04 to 0.2 wt.% and most are around 0.1 wt.% (Fig. 3c).

5.2. Composition of melt inclusion

A total of 42 melt inclusions in 42 olivine crystals were analyzed in this study. There is a negative correlation between FeO contents of the melt inclusions and Fo contents of the olivine hosts (Fig. 5), which is considered to be a result of Fe-loss, a common process caused by re-equilibration between melt inclusions and their olivine hosts (Danyushevsky et al., 2000). The texture that olivine grains are enclosed in coarse-grained clinopyroxene and plagioclase (Fig. 2b) indicates olivine crystallized earlier than clinopyroxene and plagioclase for the Nantianwan olivine gabbro. This means the compositions of melt inclusions captured by olivine are free from the influence of clinopyroxene and plagioclase crystallization. Hence the effect of Fe-loss and post-crystallization on the compositions of the melt inclusions are corrected using a widely applied method (Danyushevsky et al., 2000; Ford et al., 1983). In the correction, the total FeO content of the initial trapped melt is assumed to be 11.4 wt.%, which was estimated from total FeO fractionation trend of the Emeishan picrites (Kamenetsky et al., 2012; Zhang et al., 2013). After correction, the melt inclusions have SiO_2 contents ranging from 46.8 to 57.3 wt.%, MgO from 9.6 to 15.6 wt.%,

Table 1
The major element compositions of olivines from the Nantianwan intrusion.

Sample no.	SiO_2	FeO	MnO	MgO	CaO	NiO	Total	Fo	Ni
	(wt.%)							(mol%)	(ppm)
NT-12-1	42.45	11.56	0.17	44.70	0.10	0.21	99.18	87.3	1627
NT-22-1	40.15	14.28	0.20	45.47	0.08	0.26	100.43	85.0	2027
NT-23-1-1	40.37	15.00	0.21	44.32	0.07	0.27	100.25	84.0	2137
NT-23-1-2	40.19	14.51	0.21	44.55	0.06	0.28	99.79	84.5	2169
NT-23-1-3	40.12	15.25	0.21	43.62	0.09	0.27	99.55	83.6	2137
NT-23-1-4	40.51	14.95	0.20	44.06	0.08	0.28	100.07	84.0	2177
NT-23-1-5	40.13	15.26	0.21	43.25	0.08	0.30	99.22	83.5	2326
NT-23-2-1	39.40	13.13	0.17	45.78	0.09	0.22	98.79	86.1	1690
NT-23-2-2	39.88	13.03	0.18	46.23	0.14	0.17	99.63	86.3	1367
NT-23-2-3	38.23	12.28	0.13	48.08	0.06	0.15	98.93	87.5	1202
NT-23-2-4	42.31	11.89	0.15	45.68	0.04	0.13	100.16	87.3	982
NT-23-2-5	42.66	10.65	0.12	45.55	0.07	0.12	99.17	88.4	943
NT-24-1	38.84	15.15	0.21	45.47	0.10	0.28	100.04	84.3	2200
NT-24-2	39.26	14.39	0.21	45.59	0.09	0.26	99.81	85.0	2027
NT-25-1-1	40.67	13.31	0.19	44.39	0.06	0.26	98.88	85.6	2027
NT-25-1-2	42.00	12.77	0.18	44.07	0.10	0.24	99.35	86.0	1862
NT-25-1-3	39.58	11.86	0.17	47.82	0.09	0.24	99.75	87.8	1847
NT-25-1-4	41.08	13.03	0.17	45.61	0.09	0.25	100.23	86.2	1996
NT-25-15	39.33	12.85	0.18	46.68	0.09	0.24	99.38	86.6	1917
NT-25-1-5	40.64	13.63	0.18	43.98	0.07	0.26	98.76	85.2	2075
NT-25-1-6	39.91	13.00	0.18	45.60	0.06	0.25	99.00	86.2	1949
NT-25-1-7	39.99	13.87	0.19	45.56	0.07	0.25	99.93	85.4	1972
NT-25-2-1	40.08	13.56	0.18	45.85	0.09	0.28	100.03	85.8	2208
NT-25-2-2	40.08	13.53	0.19	45.76	0.11	0.26	99.91	85.8	2012
NT-25-2-3	40.07	13.72	0.19	45.74	0.10	0.26	100.08	85.6	2075
NT-25-2-4	40.08	14.63	0.21	43.51	0.11	0.27	98.81	84.1	2122
NT-25-2-5	40.16	13.90	0.20	44.94	0.07	0.28	99.55	85.2	2208
NT-25-2-6	40.18	14.04	0.20	45.14	0.11	0.27	99.93	85.1	2098
NT-25-2-7	40.02	14.17	0.20	45.32	0.11	0.27	100.09	85.1	2145
NT-26-1-1	40.39	14.16	0.19	44.00	0.07	0.28	99.09	84.7	2177
NT-26-1-2	39.87	13.82	0.19	45.35	0.04	0.28	99.54	85.4	2177
NT-26-1-3	39.63	13.13	0.18	45.73	0.09	0.26	99.02	86.1	2020
NT-26-1-4	39.97	13.58	0.18	46.14	0.09	0.27	100.24	85.8	2137
NT-26-15	40.13	13.31	0.19	44.87	0.13	0.27	98.91	85.7	2137
NT-26-1-5	39.97	14.16	0.19	44.69	0.07	0.27	99.36	84.9	2137
NT-26-16	39.66	14.20	0.20	44.61	0.09	0.26	99.03	84.9	2075
NT-26-1-7	39.88	13.71	0.18	45.52	0.07	0.26	99.62	85.5	2067
NT-26-2-1	40.92	11.83	0.15	46.36	0.12	0.16	99.53	87.5	1265
NT-26-2-2	38.54	11.61	0.17	49.49	0.08	0.21	100.09	88.4	1642
NT-26-2-3	39.63	10.52	0.14	48.59	0.07	0.20	99.12	89.2	1548
NT-26-2-4	38.66	11.25	0.13	48.52	0.10	0.15	98.81	88.5	1155
NT-26-2-5	38.77	11.02	0.14	48.60	0.06	0.13	98.68	88.7	990
NT-26-2-6	39.25	13.69	0.20	45.27	0.10	0.27	98.77	85.5	2082
NT-26-2-7	38.91	13.11	0.19	47.61	0.13	0.24	100.19	86.6	1917
NT-26-2-8	38.58	13.21	0.18	46.84	0.08	0.24	99.13	86.3	1847
NT-28-1	42.64	11.82	0.17	44.89	0.10	0.21	99.83	87.1	1619
NT-28-2	39.86	12.41	0.18	46.83	0.07	0.21	99.56	87.1	1674
NT-28-3	40.16	12.98	0.18	45.70	0.07	0.24	99.33	86.3	1886
NT-28-6	39.49	11.76	0.17	47.43	0.08	0.20	99.13	87.8	1579
NT-29-1	40.69	14.54	0.21	44.44	0.13	0.24	100.24	84.5	1847
NT-29-2	39.85	14.63	0.20	43.65	0.14	0.24	98.70	84.2	1847
NT-29-3	39.93	14.42	0.20	45.24	0.08	0.25	100.11	84.8	1925
NT-29-4	39.82	14.31	0.19	45.50	0.09	0.23	100.14	85.0	1831

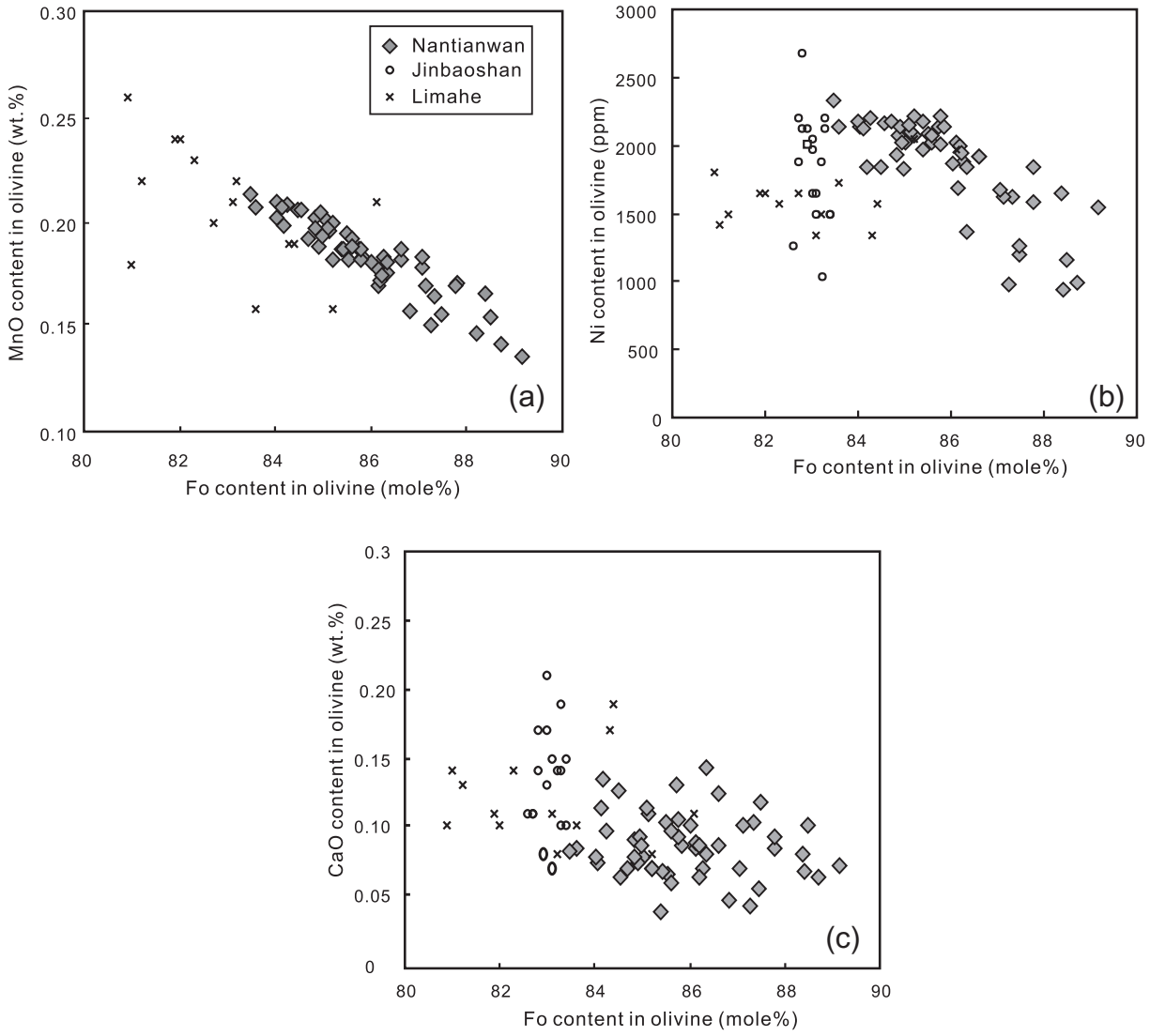

Fig. 3. Plots of MnO (a), Ni (b) and CaO (c) vs Fo for olivine of the Nantianwan intrusion. Note that Ni shows a negative correlation with Fo content. The data for Jinbaoshan and Limahe are from Tao et al. (2010) and Tao et al. (2008).

and TiO_2 from 0.36 to 2.19 wt.% (Table 2). They show tholeiitic affinity in the plot of SiO_2 versus $K_2O + Na_2O$ (Fig. 6), consistent with those for the low-Ti series in the previous studies (Xu et al., 2001; Xiao et al., 2004; Wang et al., 2007).

The melt inclusions have MgO negatively correlated with SiO_2 and Al_2O_3 (Fig. 7a and c). They have scattered CaO/Al_2O_3 against MgO (Fig. 7b). Most melt inclusions have MgO and TiO_2 contents within the range of the intermediate-Ti Emeishan flood basalts (Fig. 7d). The melt inclusion (NT-26-2-5) in the most Mg-rich olivine has 50.9 wt.% SiO_2, 15.1 wt.% MgO and 1.03 wt.% TiO_2 (Fig. 7 and Table 2).

5.3. Pb isotopic compositions of melt inclusion and plagioclase

After age correction to 260 Ma, 12 melt inclusions in the olivine crystals from olivine gabbro have $^{208}Pb/^{206}Pb$ of 2.0567–2.1032 and $^{207}Pb/^{206}Pb$ of 0.8287–0.8481, whereas 17 plagioclase grains from olivine gabbro and the transitional zone have $^{208}Pb/^{206}Pb$ of 2.0761–2.1349 and $^{207}Pb/^{206}Pb$ of 0.8373–0.8681 (Table 3). The plagioclase in the transitional zone has more radiogenetic Pb isotopic compositions than that of in olivine gabbro zone (Fig. 8).

6. Discussion

6.1. Olivine phenocrysts, xenocrysts or antecrysts?

Olivine crystals in a rock may have several origins including mantle-derived xenocrysts, antecrysts and phenocrysts crystallized from magma. Mantle-derived xenocrysts, which are remains during mantle partial melting, may be captured by upwelling magma. Because xenocrysts experience heavy deformation in mantle, they are normally anhedral and have kink band (e.g. Green and Radcliffe, 1972). However, the olivines measured in this study do not show significant deformation and generally appear with euhedral and subhedral shapes (Fig. 2b; Fig. 2 in Wang et al. (2012a)) and the abundant melt inclusions in these olivines also indicates that their olivine host are not xenocrysts. Antecrysts have a magmatic origin, but they did not crystallize from their magma host, which means antecrysts and their magma host may have no genetic connection. In this study, all the measured olivines show continuous compositional variations (Figs. 3, 5 and 7) and it seems that all these olivines share the same trends of evolution. Thus, we conclude that all the measured olivines in this study are cogenetic and are phenocrysts.

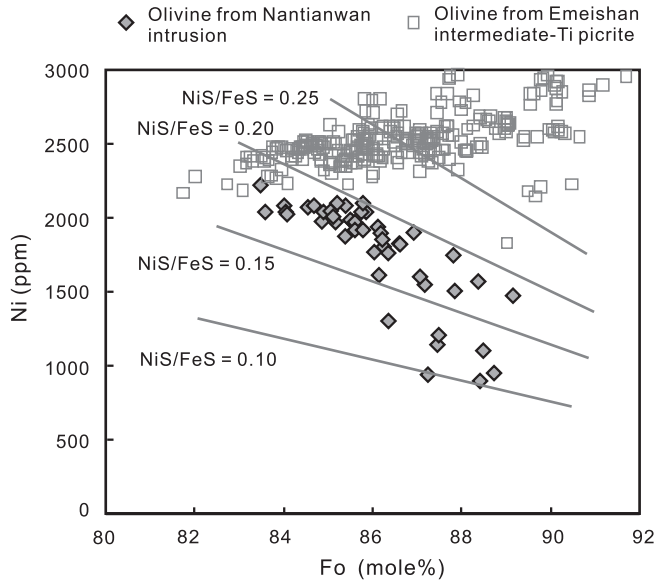

Fig. 4. Modeling of compositional variations in olivine and coexisting sulfide liquids as a result of Fe-Ni exchange between the two phases. K_D $((NiS/FeS)^{sulfide}/(NiO/FeO)^{olivine})$ was set to 10 according to Li et al. (2004). The numbers represent the NiS/FeS ratio of the re-equilibrated sulfide. The data for olivine from the intermediate-Ti picrite is from Kamenetsky et al. (2012), which is used to show the trend of normal fractional crystallization.

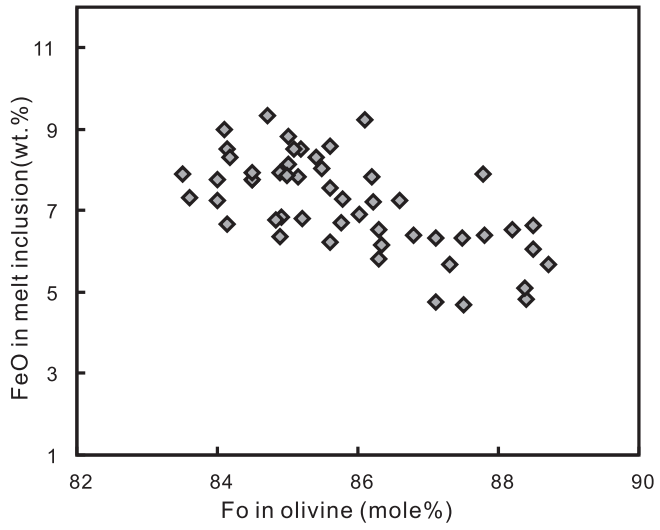

Fig. 5. The plot of FeO contents of melt inclusions in Nantianwan intrusion against Fo values of their host olivine. "Fe-loss" is expressed as a slightly negative relationship.

6.2. Possible processes that may change the compositions of melt inclusions

During and after the formation of melt inclusions, several processes may change the compositions of the trapped inclusions relative to the parental magma, including boundary layer formation, post entrapment crystallization, overheating during homogenization of melt inclusions, and re-equilibration with host crystals (Kent, 2008). The effects of these processes on the melt inclusions should be evaluated before we can use the obtained data in this study with confidence.

When a crystal grows, a boundary layer around the crystal may have formed and would be enriched in incompatible elements such as Ca, K, Th and U, and depleted in compatible elements such as Mg and Ni (Kent, 2008). If the boundary layer is thick ($\gg$10 μm) and melt inclusions are trapped rapidly in the crystal, the trapped melt inclusion may have compositions deviated from the liquid line of descent (Kent, 2008). However, it is reported that only very small melt inclusions (<15 μm in diameter) would be affected by the boundary layers (Kuzmin and Sobolev, 2004). To avoid this effect, the melt inclusions that are more than 30 μm in diameter were chosen in this study. Therefore, the effect of boundary layer should be negligible on the melt inclusions in this study.

Overheating during the homogenization of crystallized melt inclusions often leads to the interaction between the melt inclusion and host crystal. In this study, the overheating effect was compensated by iteratively subtracting a composition of olivine that is in equilibrium with the melt inclusion until the calculated composition of the melt inclusion is in equilibration with its host (cf. Danyushevsky et al., 2000).

Diffusive exchange (re-equilibration) between the melt inclusion and the host olivine may bias the compositions of melt inclusion, resulting in the "Fe-loss" from the melt inclusion (e.g. Danyushevsky et al., 2000). The Fe-loss effect in this study is resolved using a well-known Fe-loss correction program, which adopts a target FeO^* based on the olivine fractionation trend of bulk compositions of the host rocks (Danyushevsky et al., 2000).

In this study, we analyzed the Pb isotopic ratios of the melt inclusions in the olivine and the plagioclase in both olivine gabbro and transitional zone (Table 3). As shown in Fig. 8, the melt inclusions in the olivine have $^{208}Pb/^{206}Pb$ and $^{207}Pb/^{206}Pb$ ratios similar to the range of the Emeishan flood basalts, whereas the plagioclase in the olivine gabbro and the transitional zone have the Pb isotopic ratios ranging from those for the Emeishan flood basalts to that for the basement of the Yangtze Block (Zhang et al., 1997). Given that the olivine gabbro samples also have restricted and low γOs values (+5 to +15) (Wang et al., 2012a), the melt inclusions in the most Mg-rich olivine crystal from the olivine gabbro may have preserved the information of the least evolved parental magma of the Nantianwan intrusion. This is supported by the fact that the melt inclusions have nearly constant $^{208}Pb/^{206}Pb$ and $^{207}Pb/^{206}Pb$ ratios with the fractionation of the magma (Fig. 9). Because if the olivine gabbro had endured crustal contamination, the lead isotopic ratios of the melt inclusions may show correlations with their major elemental contents. Therefore, we consider that the melt inclusion hosted in the most Mg-rich olivine in this study may preserve the compositions of the least evolved parental magma of the Nantianwan intrusion on the liquid line of descent.

6.3. Re-equilibration between olivine and sulfide

There is a negative correlation between Ni and Fo for the olivine crystals in the Nantianwan intrusion, which is different from a positive correlation for the olivine crystals in many volcanic rocks (e.g. Liu et al., 2015; Qian et al., 2015). The negative correlation of Ni and Fo for the olivine crystals is explained as the Fe-Ni exchange between olivine crystals and concurrent sulfide liquid (Li et al., 2004, 2007). The sulfides are visible in the olivine gabbro (Wang et al., 2012a, Fig. 2e and f) so that the olivine may have experienced Fe-Ni exchange reaction with the sulfide liquids before complete solidification. Ni and Fe will exchange between olivine and sulfide liquid according to the reaction:

$$NiO^{olivine} + FeS^{sulfide} = NiS^{sulfide} + FeO^{olivine} \quad (1)$$

The exchange partition coefficient K_D for this reaction is defined as:

$$K_D = (NiS/FeS)^{sulfide}/(NiO/FeO)^{olivine} \quad (2)$$

Table 2
The major element compositions of olivine-hosted melt inclusions from the Nantianwan intrusion (after Fe-loss correction).

	SiO_2	TiO_2	Al_2O_3	Fe_2O_3	FeO	MnO	MgO	CaO	Na_2O	K_2O	P_2O_5	NiO	Fo
	wt.%												(mol%)
NT-23-1-1	48.93	0.57	13.01	1.29	10.47	0.18	9.55	13.67	1.88	0.42	0.05	0.12	84
NT-23-1-2	56.42	1.31	11.47	1.29	10.48	0.13	11.49	4.87	1.76	0.56	0.22	0.02	84.5
NT-23-1-3	56.56	1.34	11.85	1.29	10.48	0.09	10.62	5.27	2.00	0.44	0.05	0.05	83.6
NT-23-1-4	53.16	2.19	9.91	1.29	10.47	0.18	10.27	9.50	2.18	0.40	0.45	0.07	84
NT-23-1-5	54.95	1.20	11.94	1.29	10.48	0.15	10.40	7.19	1.84	0.44	0.12	0.00	83.5
NT-23-2-1	50.19	1.41	10.48	1.29	10.47	0.22	11.30	12.07	2.15	0.31	0.12	0.18	86.1
NT-23-2-2	52.62	0.83	10.86	1.29	10.47	0.10	12.18	8.95	2.17	0.43	0.10	0.01	86.3
NT-23-2-3	49.34	0.36	13.93	1.29	10.47	0.08	12.92	8.79	2.28	0.47	0.07	0.02	87.5
NT-24-1	56.96	1.40	9.56	1.29	10.47	0.20	11.76	5.43	2.12	0.65	0.16	0.13	85
NT-25-1-1	51.30	1.15	10.67	1.29	10.48	0.12	10.80	11.25	2.45	0.35	0.13	0.00	85.6
NT-25-1-2	53.07	1.02	11.43	1.29	10.48	0.11	12.23	7.98	1.84	0.38	0.18	0.02	86
NT-25-1-3	54.27	1.01	9.31	1.29	10.47	0.20	14.12	6.07	2.66	0.55	0.05	0.15	87.8
NT-25-1-4	55.62	1.02	10.36	1.29	10.47	0.20	13.59	6.57	0.29	0.51	0.08	0.14	86.2
NT-25-15	57.30	1.12	10.57	1.29	10.48	0.17	14.28	3.14	0.91	0.64	0.11	0.08	86.6
NT-25-1-5	55.24	1.46	9.55	1.29	10.47	0.25	11.22	6.64	3.12	0.69	0.09	0.21	85.2
NT-25-1-6	55.33	1.07	9.82	1.29	10.48	0.11	12.53	6.23	2.42	0.64	0.07	0.05	86.2
NT-25-2-1	53.42	1.03	11.73	1.29	10.48	0.11	12.02	7.25	2.13	0.39	0.14	0.02	85.8
NT-25-2-2	54.07	0.96	10.93	1.29	10.48	0.13	12.03	7.35	2.28	0.38	0.11	0.01	85.8
NT-25-2-3	53.16	1.40	12.54	1.29	10.48	0.10	11.72	6.29	2.30	0.55	0.18	0.22	85.6
NT-25-2-4	52.94	1.10	12.60	1.29	10.48	0.11	10.25	7.91	2.59	0.61	0.12	0.17	84.1
NT-25-2-5	57.08	1.68	11.33	1.30	10.49	0.10	12.26	3.38	1.73	0.51	0.16	0.03	85.2
NT-25-2-6	54.41	0.42	10.16	1.29	10.48	0.21	11.46	8.75	2.15	0.44	0.23	0.16	85.1
NT-25-2-7	54.18	0.57	10.39	1.29	10.47	0.30	10.98	7.91	3.22	0.63	0.06	0.18	85.1
NT-26-1-1	53.18	2.15	11.85	1.29	10.48	0.17	10.66	7.17	2.93	0.08	0.04	0.02	84.7
NT-26-1-5	55.57	1.47	11.37	1.29	10.47	0.13	11.24	4.87	2.44	1.09	0.06	0.13	84.9
NT-26-16A	54.38	1.20	12.45	1.29	10.48	0.25	11.32	5.57	2.40	0.48	0.19	0.14	84.9
NT-26-16B	54.32	1.69	12.23	1.29	10.47	0.15	11.67	6.25	1.25	0.54	0.15		84.9
NT-26-2-1	51.82	1.11	9.31	1.29	10.48	0.12	13.39	10.40	1.58	0.37	0.13	0.00	87.5
NT-26-2-2	51.36	0.86	10.37	1.29	10.48	0.09	14.48	8.62	1.87	0.52	0.06	0.03	88.4
NT-26-2-4	51.03	0.89	10.97	1.29	10.48	0.11	14.53	7.78	2.28	0.46	0.18	0.03	88.5
NT-26-2-5	50.88	1.03	9.52	1.29	10.47	0.11	15.06	8.58	2.33	0.53	0.20	0.03	88.7
NT-26-2-6	51.48	0.86	13.51	1.29	10.47	0.24	11.35	8.03	2.24	0.50	0.03	0.12	85.5
NT-26-2-8	52.35	1.27	12.31	1.29	10.47	0.12	12.07	6.36	2.41	1.18	0.17	0.07	86.3
NT-28-1	55.59	0.86	9.88	1.29	10.48	0.07	13.51	4.24	2.15	1.86	0.07	0.06	87.1
NT-28-2	50.31	1.64	10.03	1.29	10.48	0.12	12.02	10.83	2.57	0.54	0.17	0.03	87.1
NT-28-3	55.70	1.44	10.90	1.29	10.48	0.10	13.24	4.71	1.57	0.46	0.12	0.03	86.3
NT-28-6	54.65	1.69	10.19	1.29	10.48	0.11	15.06	4.74	1.25	0.41	0.11	0.00	87.8
NT-29-1a	55.72	0.43	12.14	1.29	10.47	0.24	10.91	5.64	2.48	0.51	0.17	0.10	84.2
NT-29-1b	54.67	0.98	11.45	1.30	10.49	0.12	11.25	7.68	1.55	0.41	0.10	0.01	84.5
NT-29-2	53.68	0.97	11.89	1.30	10.50	0.15	10.95	8.12	1.98	0.36	0.11		84.5
NT-29-3	55.91	1.28	11.20	1.29	10.47	0.11	11.47	5.52	2.18	0.46	0.13	0.04	84.8
NT-29-4	54.99	1.21	11.53	1.30	10.49	0.12	11.57	6.16	2.08	0.45	0.11	0.01	85

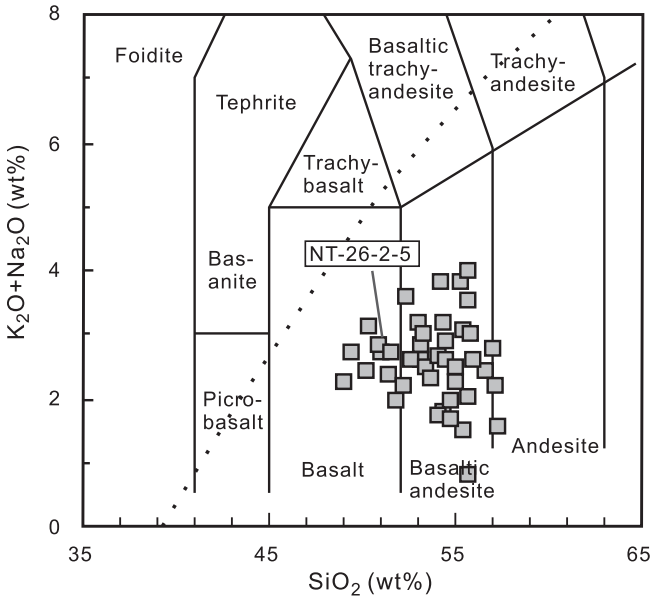

Fig. 6. TAS rock classification diagram after Le Bas et al. (1986) for melt inclusions from the Nantianwan intrusion. The compositions of melt inclusions are corrected for Fe-loss (see text further explanation).

Change Eq. (2) to the following form,

$$(NiO)^{olivine} = (FeO)^{olivine} * (NiS/FeS)^{sulfide}/K_D \quad (3)$$

K_D is constant at constant fO_2 and sulfide liquid composition (Brenan, 2003). Therefore, the olivine with elevated FeO will contain more Ni than the olivine with low FeO so that Ni would be negatively correlated with Fo. Using the Emeishan immediate-Ti picrite as an end-member and Eq. (2), the Ni-Fe ratio of the coexisting sulfide liquids can be estimated and shown in Fig. 4. Most olivine crystals from the Nantianwan intrusion are plotted between the trend line with NiS/FeS of 0.15 and the line of 0.20. The Ni contents of melt inclusions also have a weak negative correlation with the Fo contents of the host olivine (not shown) indicating at least the Ni contents of melt inclusions were altered by the re-equilibration. However, only the contents of these trace elements which are compatible in both olivine and sulfide (e.g. Ni) would change and the contents of major elements would almost keep constant.

6.4. Parental magma compositions based on melt inclusion in olivine

Different ways have been tried to estimate the compositions of the parental magmas of the Ni-Cu-(PGE) sulfide-bearing mafic-ultramafic intrusions in the Emeishan LIP. The Limahe intrusion is estimated to have formed from a parental magma with MgO of 16.7 wt.% and CaO/Al_2O_3 of 0.96 (Tao et al., 2007a). Tao et al.

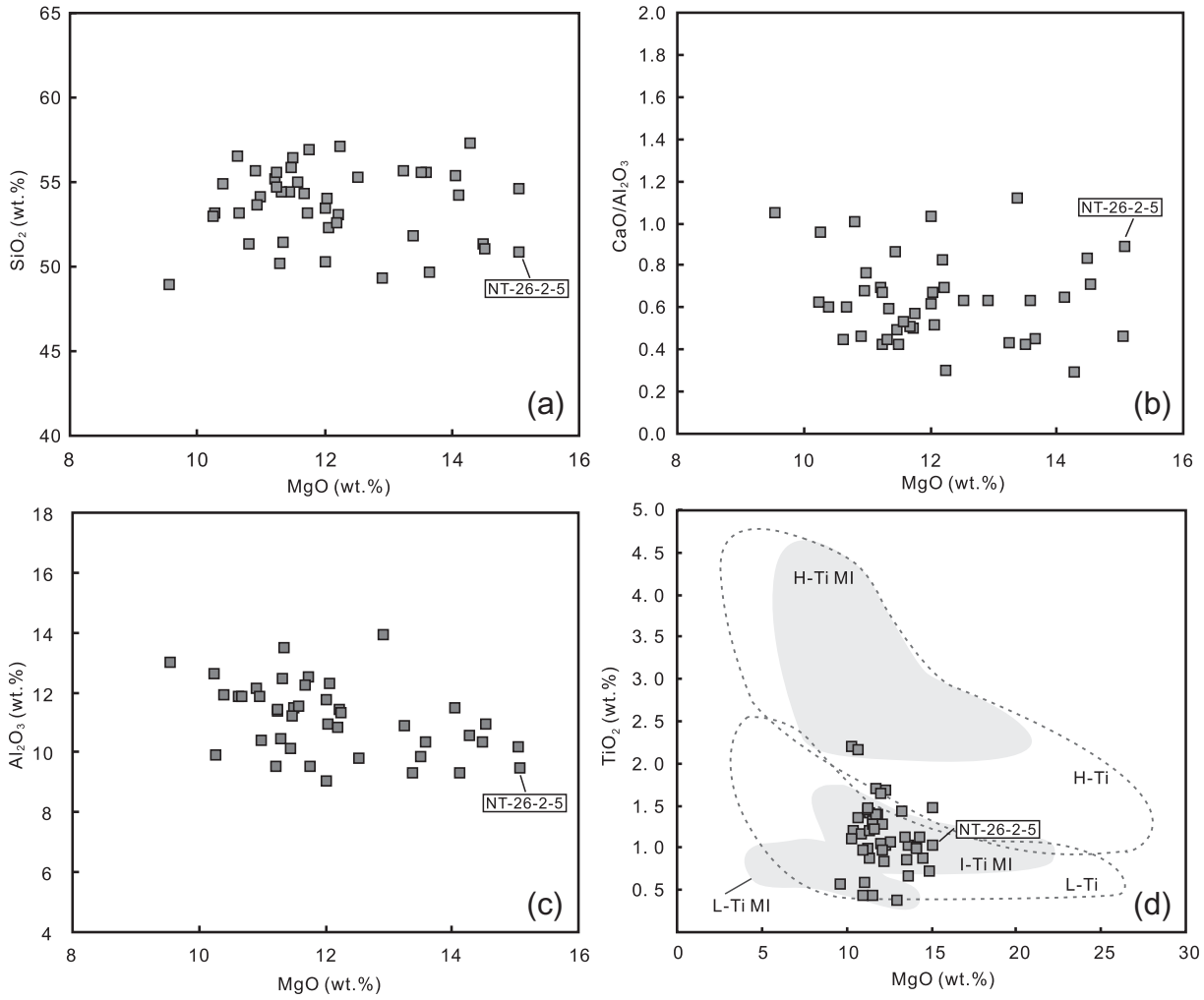

Fig. 7. Major element contents and their ratios against MgO variation diagrams for melt inclusions of the Nantianwan intrusion after correction for Fe-loss: (a), SiO_2 vs MgO; (b), CaO/Al_2O_3 vs MgO; (c), Al_2O_3 vs MgO; (d), TiO_2 vs MgO. The gray dashed lines show the high-Ti (H-Ti) and low-Ti (L-Ti) magma series classified according to Xu et al. (2001). The data source: High-Ti series are from Chung and Jahn (1995), Xu et al. (2001, 2007), Song et al. (2006), Zhang et al. (2006), Wang et al. (2007), and Hanski et al. (2010). Low-Ti series are from Xu et al. (2001), Song et al. (2006), Wang et al. (2007), Hanski et al. (2010) and Kamenetsky et al. (2012). The shadowed areas show the low-Ti melt inclusion (L-Ti MI), intermediate-Ti melt inclusion (I-Ti MI) and high-Ti melt inclusion (H-Ti MI) from Kamenetsky et al. (2012). The lack of significant correlation between CaO/Al_2O_3 and MgO indicates olivine was the only crystallized phase.

(2008) further compared the Limahe intrusion with the Emeishan picrites in terms of trace element and chalcophile element patterns and concluded that the parental magma of the Limahe intrusion has compositions similar to that of the Emeishan picrite. Zhu et al. (2011) considered that the Qingkuangshan Ni-Cu-(PGE) sulfide deposit formed from a picritic magma because the intrusion has bulk compositions similar to that of the Limahe intrusion. However, the available data indicate that the Fo contents of the olivine in all of these intrusions are less than 86 (Wang et al., 2005; Tao et al., 2008), indicating that the parental magma of these Ni-Cu-(PGE) sulfide-bearing intrusions is far from primitive. Wang et al. (2005) calculated the Al_2O_3 content and MgO/FeO ratio of the parental magma of the Jinbaoshan intrusion based on the compositions of Cr-spinel and olivine in the intrusion and concluded that the parental magma is a high-Mg tholeiitic melt. In a previous study on the Nantianwan intrusion, the melt from which the most Mg-rich olivine (Fo = 86) crystallized was estimated to have an MgO content of ~8.2 wt.% with a FeO/MgO ratio of 0.65 (Wang et al., 2012a). Wang et al. (2012a) considered that the estimated MgO content is likely to be a minimum because the observed olivine composition may have been affected by subsequent re-equilibration with trapped silicate liquid, a process that can reduce the Fo contents (e.g., Li et al., 2004). Therefore, the parental magma of the olivine gabbros may have >8.2 wt.% MgO, which is within the range of high-Mg basaltic magma. However, the exact MgO value cannot be obtained by this method at that time.

In this study, the most Mg-rich olivine has Fo of 89, using Mg-Fe exchange coefficient of 0.3 between olivine and melt (Roeder and Emslie, 1970) and the FeO content of parental magma of ~10.5 wt.%, which is estimated from the Emeishan LIP picrites (Kamenetsky et al., 2012; Zhang et al., 2013), the calculated MgO content of the parental magma is ~14.3 wt.%. On the other hand, the melt inclusion (NT-26-2-5) in the most Mg-rich olivine (Fo = 89) in this study contain SiO_2 of 50.9 wt.%, MgO of 15.1 wt.%, TiO_2 of 1.0 wt.% and CaO/Al_2O_3 of 0.90 (Fig. 7 and Table 2). The MgO value of the melt inclusion from the most Mg-rich olivine is nearly identical to the estimated value based on Mg-Fe exchange in the most Mg-rich olivine. The relatively low MgO value in the estimation may be related to the selection for the Mg-Fe exchange coefficient. We therefore treat the composition of the melt inclusion enclosed in the most Mg-rich olivine as the parental magma of the Nantianwan intrusion.

Xu et al. (2001) first divided the Emeishan basalts into low-Ti and high-Ti series based on Ti/Y ratio of 500. Xiao et al. (2004)

Table 3
The Pb isotope composition of melt inclusions and plagioclases from the Nantianwan intrusion.

		$^{208}Pb/^{206}Pb_i$	SE	$^{207}Pb/^{206}Pb_i$	SE
Melt inclusion	NT-23-1-1	2.0931	0.0039	0.8410	0.0015
	NT-23-1-4	2.0780	0.0011	0.8386	0.0006
	NT-23-1-5	2.0567	0.0014	0.8295	0.0007
	NT-23-2-1	2.0796	0.0024	0.8413	0.0010
	NT-23-2-2	2.0939	0.0040	0.8385	0.0018
	NT-25-1-1	2.0592	0.0047	0.8287	0.0019
	NT-25-1-2	2.0842	0.0056	0.8360	0.0028
	NT-25-1-3	2.0732	0.0020	0.8326	0.0010
	NT-25-1-4	2.0772	0.0018	0.8381	0.0009
	NT-25-2-1	2.0929	0.0028	0.8425	0.0013
	NT-25-2-3	2.0950	0.0036	0.8409	0.0015
	NT-25-2-4	2.1032	0.0022	0.8481	0.0012
Plagioclase	NT-Pl-26-1	2.0817	0.0021	0.8381	0.0011
	NT-Pl-26-2	2.0761	0.0025	0.8373	0.0010
	NT-Pl-26-3	2.0880	0.0018	0.8416	0.0009
	NT-Pl-26-4	2.0818	0.0013	0.8406	0.0006
	NT-Pl-26-5	2.0812	0.0025	0.8383	0.0010
	NT-Pl-26-6	2.0852	0.0025	0.8398	0.0013
	NT-Pl-38-1	2.1209	0.0023	0.8649	0.0010
	NT-Pl-38-2	2.1163	0.0023	0.8620	0.0011
	NT-Pl-38-3	2.1229	0.0023	0.8680	0.0012
	NT-Pl-38-4	2.1166	0.0019	0.8643	0.0010
	NT-Pl-40-1	2.1229	0.0024	0.8635	0.0011
	NT-Pl-40-2	2.1303	0.0043	0.8681	0.0022
	NT-Pl-40-3	2.1349	0.0045	0.8667	0.0024
	NT-Pl-40-4	2.1290	0.0038	0.8652	0.0023
	NT-Pl-40-5	2.1191	0.0019	0.8616	0.0009
	NT-Pl-40-6	2.1099	0.0015	0.8596	0.0007
	NT-Pl-40-7	2.1111	0.0015	0.8593	0.0006
Standard (n = 18)	BHVO-2G	2.0549		0.8337	
	Accuracy	0.12%		−0.09%	
	2RSD	0.16%		0.19%	

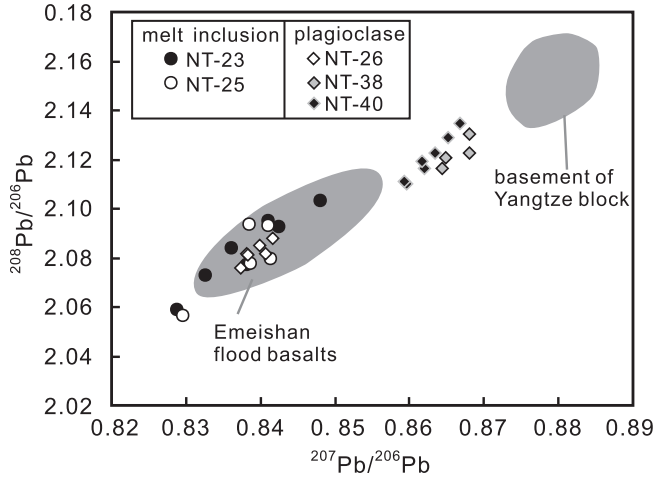

Fig. 8. Pb isotope of melt inclusions and plagioclases from the Nantianwan intrusion. NT-23, NT-25 and NT-26 were collected from the lower zone. NT-38 and NT-40 were from the transitional zone. NT-23 and NT-25 are melt inclusions and the others are plagioclases. The Pb isotopic ratios of the Emeishan flood basalts are from Zhang et al. (2006), Xu et al. (2007) and Ren et al. unpublished data. The data of basement of Yangtze block is from Zhang et al. (1997).

found a compositional gap between low-Ti and high-Ti basalts in the Binchuan section. Zhou et al. (2008) studied several ore-bearing intrusions in the Emeishan LIP and concluded that the giant Fe-Ti-V oxide ore deposits were derived from high-Ti magma and the Ni-Cu sulfide deposits were derived from low-Ti magma. However, more and more recent studies suggested that the Emeishan basalts have continuous compositions and there is no compositional gap between low-Ti and high-Ti basalts (e.g. Hou et al., 2011; Shellnutt and Jahn, 2011; Kamenetsky et al., 2012), which means a reevaluation of the relationship between ore deposits and the Emeishan basalts is needed. Kamenetsky et al. (2012) divided the Emeishan basalts into low-Ti, intermediate-Ti and high-Ti series. Most of the Nantianwan olivine-hosted melt inclusions measured in this study have compositions within the range of the intermediate-Ti series of the Emeishan LIP (Fig. 7d). What is more, the Jinping basalts, which locate besides the Baimazhai Ni-Cu-(PGE) sulfide deposit, and the Dashibao formation basalts, which surround the Yangliuping Ni-Cu sulfide deposit have Ti/Y ratios varying from 341 to 490 (Wang et al., 2007) and from 320 to 628 (Song et al., 2006), respectively. These basalts also have intermediate-Ti-like compositions. Thus we conclude that the Ni-Cu-(PGE) sulfide deposits associate with intermediate-Ti basalts in the Emeishan LIP.

The intermediate-Ti series is composed of evolved flood basalts in the Emeishan LIP, which is considered to have been evolved from primitive picritic magma. Kamenetsky et al. (2012) reported the most Mg-rich picrite (EM43) in the Emeishan LIP with 25 wt.% MgO, 0.5 wt.% TiO_2 and CaO/Al_2O_3 of 0.98. The CaO/Al_2O_3 ratio of the melt inclusion from the most Mg-rich olivine of the Nantianwan intrusion is similar to that of the Emeishan intermediate-Ti picrite (1.0, Kamenetsky et al., 2012). At the same CaO/Al_2O_3, the melt inclusion (NT-26-2-5) has less MgO than that for EM43, indicating that the melt inclusion (NT-26-2-5) preserved an evolved melt. Wang et al. (2014) explained the Abulangdang ultramafic intrusion in the central part of the Emeishan LIP, representing the cumulate of olivine and chromite from a high-Ti picritic magma and representing the missing ultramafic portion of the Fe-Ti oxide-bearing layered intrusions in the Panxi region. We assume such a process may have also happened for the intermediate-Ti picritic magma during ascent as most Ni-Cu-(PGE) sulfide-bearing intrusions have olivine with Fo < 86 (Wang

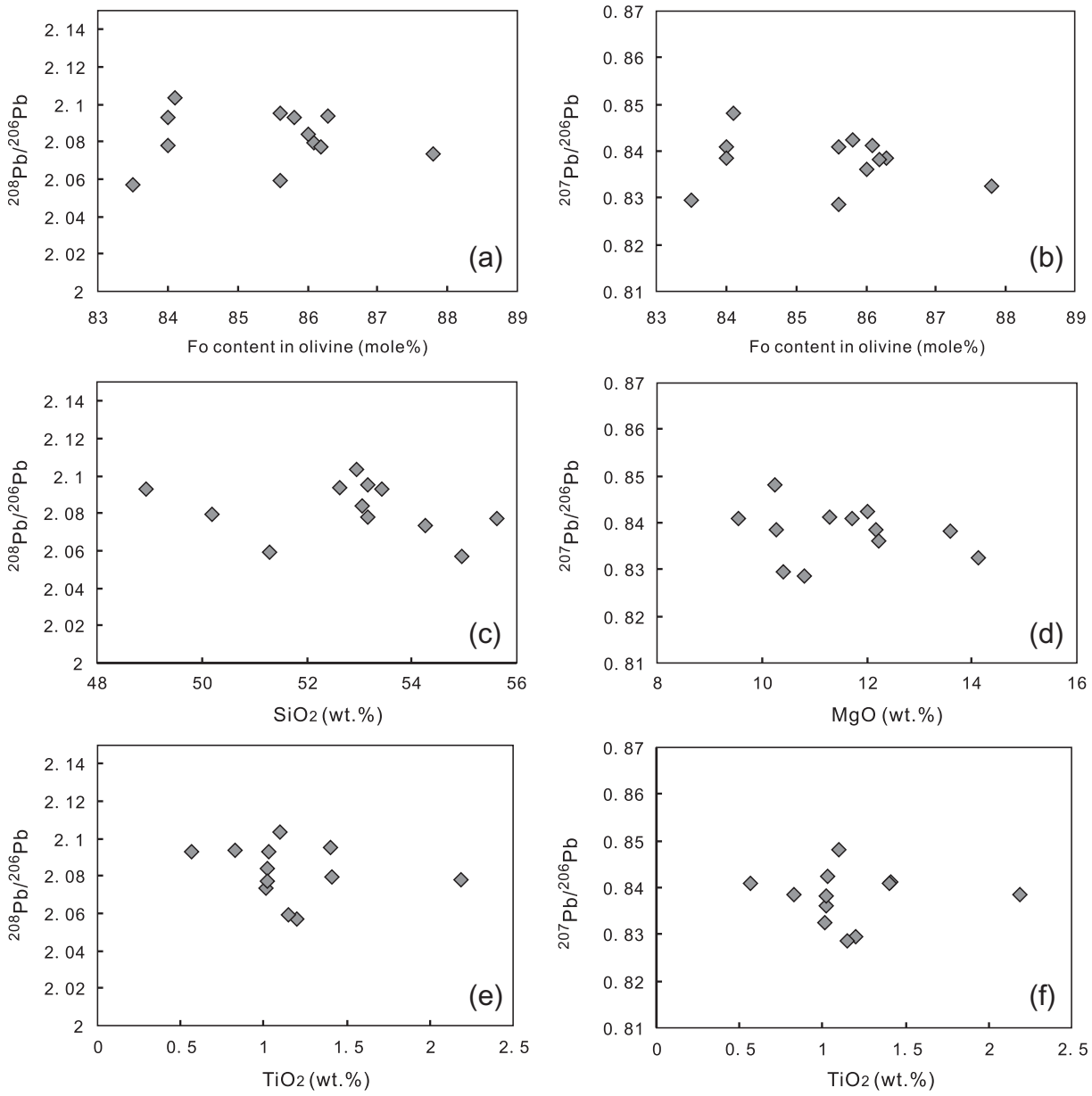

Fig. 9. (a) $^{208}Pb/^{206}Pb$ vs Fo, (b) $^{207}Pb/^{206}Pb$ vs Fo, (c) $^{208}Pb/^{206}Pb$ vs SiO_2, (d) $^{207}Pb/^{206}Pb$ vs MgO, (e) $^{208}Pb/^{206}Pb$ vs TiO_2, (f) $^{207}Pb/^{206}Pb$ vs TiO_2 for the Nantianwan melt inclusions. The Pb isotopic ratios are constant and show little correlations with Fo content or major elements.

et al., 2005; Tao et al., 2008). Therefore, the melt inclusion trapped in the most Mg-rich olivine of the Nantianwan intrusion may represent the least evolved magma before the fractionation in the shallow magma chamber.

6.5. Parental magma compositions of the Ni-Cu-(PGE) sulfide-bearing intrusions in the Emeishan LIP

The composition of the melt inclusion (NT-26-2-5) in the most Mg-rich olivine of the Nantianwan intrusion is comparable with the parental magma composition of the Limahe and Yangliuping intrusions, another two sulfide-bearing mafic intrusions in the Emeishan LIP (Table 4). Except SiO_2, the major oxides of the melt inclusion NT-26-2-5 are similar to that for the parental magma of the Limahe intrusion. Compared to the Nantianwan intrusion, the parental magma of the Yangliuping intrusion has higher CaO and lower MgO, but similar other major oxide contents. This may be caused by that the parental magma of the Yangliuping intrusion

Table 4
Chemical composition of the parental magma of the Nantianwan intrusion and the Limahe intrusion.

Element[a]	Nantianwan	Limahe[b]	Yangliuping[c]
SiO_2	50.88	47.95	49.5
TiO_2	1.03	1.89	1.8
Al_2O_3	9.52	9.66	10.3
Fe_2O_3	1.29	1.2	1.7
FeO	10.47	10.3	10.4
MnO	0.11		0.17
MgO	15.06	16.67	10.8
CaO	8.58	9.28	12
Na_2O	2.33	1.37	1.0
K_2O	0.53	0.52	2.3
P_2O_5	0.2	0.12	0.26

[a] Major oxides are reported in weight percent (wt.%).
[b] The composition of the parental magma of Limahe is from Tao et al. (2007a).
[c] The composition of the parental magma of Yangliuping is derived from the data in Wang et al. (2001) with the method of Chai and Naldrett (1992) assuming that the parental magma equilibrates with olivine having Fo of 86.

underwent more olivine crystallization fractionation. Therefore, the melt inclusion in the most Mg-rich olivine in this study can be taken as an analogue of the parental magma of other Ni-Cu-(PGE) sulfide-bearing intrusions in the Emeishan LIP.

6.6. Modeling of the crystallization sequence

Olivine was the first crystallized silicate mineral in the olivine gabbro of the Nantianwan intrusion (Wang et al., 2012a, Fig. 2a–d). The melt inclusions in the olivine are scattered without a linear trend on the plot of CaO/Al_2O_3 versus MgO (Fig. 7b), indicating that the olivine was the only crystallization phase at MgO > 10 wt.%. Using the composition of the melt inclusion in the most Mg-rich olivine as the parental magma of the Nantianwan intrusion, the crystal fractionation process is simulated using MELTS program (Ghiorso and Sack, 1995; Asimow and Ghiorso, 1998) under oxygen fugacity around quartz-fayalite-magnetite (QFM) condition (e.g. Mathez, 1984; Christie et al., 1986; Ballhaus, 1993; Mallmann and O'Neill, 2009). Under different water contents and pressures, phase diagrams for parental magma NT-26-2-5 were constructed with MELTS program (Fig. 10). Many previous studies have suggested that water has a significant effect on the crystallization sequence (e.g. Botcharnikov et al., 2008; Hong et al., 2013; Howarth et al., 2013). The modeling results indicate higher H_2O delays or even hampers orthopyroxene and plagioclase crystallization. For example, under the pressure condition of 3 kbar, if the water content is more than 1.3 wt.%, orthopyroxene will not crystallize (Fig. 10b). Because no hydrous mineral was observed in the thin sections of the Nantianwan intrusion, we set the water content of 0.5 wt.% to do the following modeling. Fig. 10d shows that under the water content of 0.5 wt.% olivine is the liquidus phase at pressure less than 5.3 kbar and if the pressure is less than 1.6 kbar, orthopyroxene will not crystallize. Combining the depth of the emplacement of the Nantianwan intrusion (~4.5–5.5 km, Wang et al., 2012b), we set the pressure to 2.0 kbar. The simulation shows that olivine began to crystallize when the temperature decreased to below 1381 °C, and that the first crystallized olivine has Fo content of 89, equal to the highest Fo of the olivine in this study (Table 5). After 17 wt.% olivine crystallized, the liquidus phase changed to orthopyroxene. When the temperature was below 1207 °C, orthopyroxene and clinopyroxene would crystallize together. The first plagioclase crystal appeared at 1124 °C. This fractionation sequence is consistent with the petrographic observation that the olivine is enclosed in both orthopyroxene and clinopyroxene and the mineral assemblage in unhomogenized melt inclusions (Fig. 2b and d). Therefore, we consider that the Nantianwan intrusion formed when the magma emplaced in a shallow magma chamber at depth of ~6 km (equivalent to 2.0 kbar). Such a process is similar to what happened in other Ni-Cu-(PGE) sulfide deposits elsewhere in the Emeishan LIP such as the Baimazhai intrusion (Wang et al., 2006) and the Limahe intrusion (Tao et al., 2008). Therefore, we conclude that the Ni-Cu-(PGE) sulfide-poor and Ni-Cu-(PGE) sulfide-rich intrusions in the Emeishan LIP may have similar parental magma and similar magma pro-

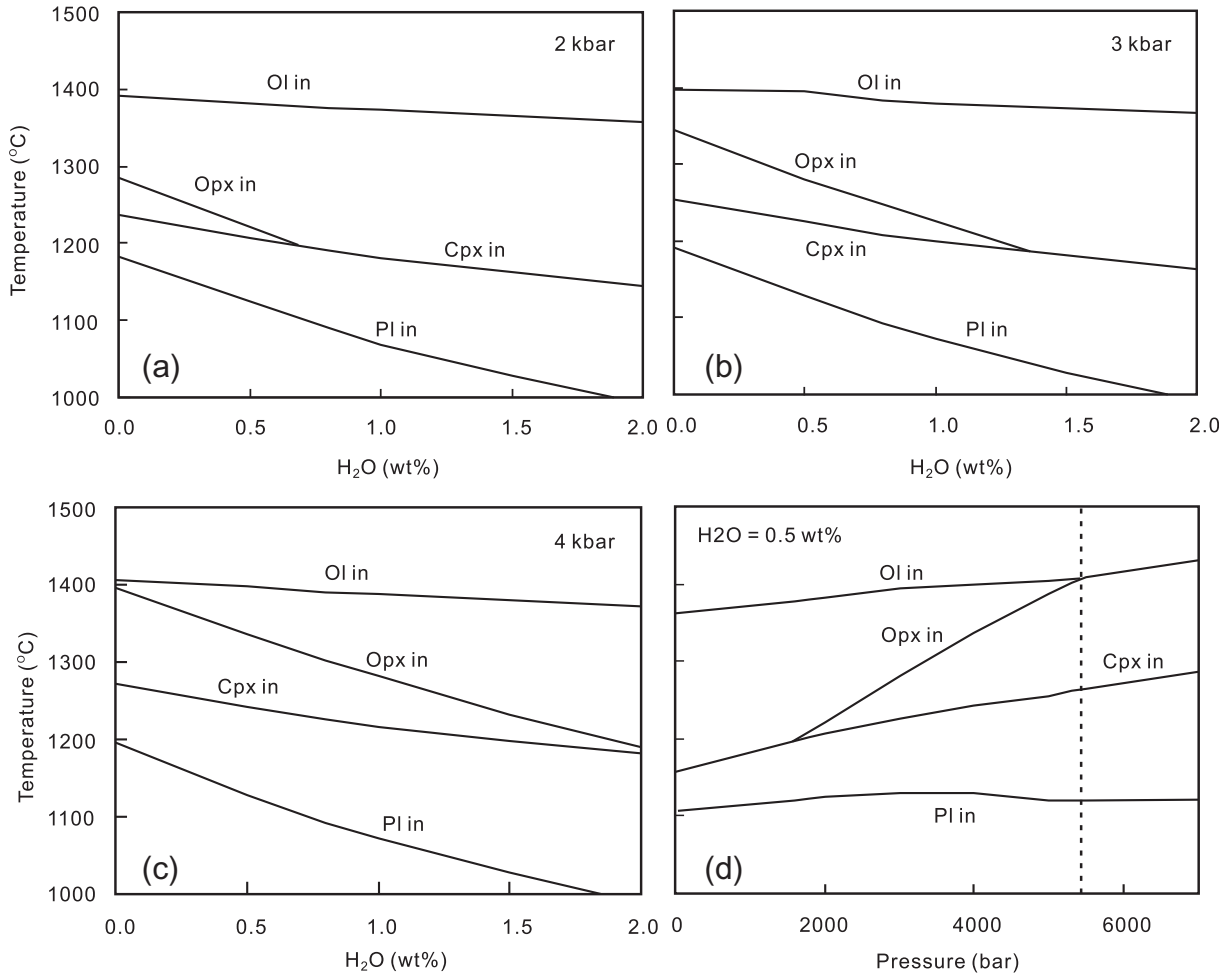

Fig. 10. Calculated phase-diagrams, simulated by MELTS program. (a)–(c) Phase equilibria with different water contents under pressure of 2 kbar (a), 3 kbar (b) and 4 kbar (c). (d) Phase equilibria as a function of pressure under water content of 0.5 wt.% (see text for discussion).

Table 5
Simulation of fractional crystallization in the shallow magma chamber based on MELTS program.[a]

	Crystals	Liquid	Evolved magma/w(B)/%										
Temperature/°C	Ol:Opx:Cpx:Pl	wt.%	SiO_2	TiO_2	Al_2O_3	Fe_2O_3	FeO	MnO	MgO	CaO	Na_2O	K_2O	P_2O_5
	0:0:0:0	100	50.88	1.03	9.52	1.29	10.47	0.11	15.06	8.58	2.33	0.53	0.20
1381	0.3:0:0:0	99.7	50.87	1.03	9.49	1.67	10.07	0.11	14.89	8.55	2.33	0.53	0.20
1221	17.1:0.2:0:0	82.7	52.83	1.26	11.51	1.81	9.70	0.12	8.20	10.30	2.82	0.64	0.24
1207	17.1:2.0:0.2:0	80.7	52.76	1.27	11.76	1.84	9.68	0.12	7.69	10.48	2.89	0.66	0.25
1124	17.1:2.0:23.0:0.3	57.6	53.16	1.64	15.01	1.93	10.46	0.14	3.75	7.81	3.96	0.92	0.35

[a] MELTS simulation parameter: pressure, 2.0 kbar; f_{O2}: QFM; H_2O, 0.5 wt.%.

cess in the magma conduit, the key factor to control the mineralization is the degrees of crustal contamination during the magma processes (Xu et al., 2014).

7. Conclusion

The melt inclusion in the most Mg-rich olivine of the Nantianwan intrusion contains 50.9 wt.% SiO_2, 15.1 wt.% MgO and 1.03 wt.% TiO_2, which can be taken as an analogue of the parental magma of the Ni-Cu-(PGE) sulfide-bearing intrusions elsewhere in the Emeishan LIP. The similarity of CaO/Al_2O_3 and lower MgO content compared to the Emeishan intermediate-Ti picrite indicates the melt inclusion may evolve from the intermediate-Ti picrite. The Ni-Cu-(PGE) sulfide-bearing mafic-ultramafic intrusions in the Emeishan LIP may have formed from evolved high-Mg, intermediate-Ti basaltic magmas, which were derived from intermediate-Ti picritic magma that experienced early crystallization of olivine at depth.

Acknowledgements

We thank Wu Lei for the kind assistance in EPMA analysis. We also gratefully acknowledge the editor Diane Chung, an anonymous reviewer, Geoffrey H. Howarth and Ping-Ping Liu for the critical and constructive comments. The study is supported by the Strategic Priority Research Program (B) of the Chinese Academy of Sciences (XDB18030601), National Science Foundation of China (41172064), National Basic Research Program of China (2011CB808903), the "hundred talent project" of Chinese Academy of Sciences.

References

Asimow, P.D., Ghiorso, M.S., 1998. Algorithmic modifications extending MELTS to calculate subsolidus phase relations. Am. Miner. 83, 1127–1132.
Ballhaus, C., 1993. Redox states of lithospheric and asthenospheric upper mantle. Contrib. Mineral. Petrol. 114, 331–348.
Bernstein, S., Kelemen, P.B., Brooks, C.K., 1996. Evolution of the Kap Edvard Holm Complex: a mafic intrusion at a rifted continental margin. J. Petrol. 37, 497–519.
Botcharnikov, R.E., Almeev, R.R., Koepke, J., 2008. Phase relations and liquid lines of descent in hydrous ferrobasalt—implications for the Skaergaard intrusion and Columbia River flood basalts. J. Petrol. 49, 1687–1727.
Boudreau, A., 1999. Fluid fluxing of cumulates: the J-M Reef and associated rocks of the Stillwater Complex, Montana. J. Petrol. 40, 755–772.
Brenan, J.M., 2003. Effects of fO_2, fS_2 temperature, and melt composition on Fe-Ni exchange between olivine and sulfide liquid: implications for natural olivine-sulfide assemblages. Geochim. Cosmochim. Acta 67, 2663–2681.
Chai, G., Naldrett, A.J., 1992. The Jinchuan ultramafic intrusion: cumulate of a high-Mg basaltic magma. J. Petrol. 33, 277–303.
Chalokwu, C.I., Grant, N.K., Ariskin, A.A., Barmina, G.S., 1993. Simulation of primary phase relations and mineral compositions in the Partridge River intrusion, Duluth Complex, Minnesota: implications for the present magma composition. Contrib. Mineral. Petrol. 114, 539–549.
Christie, D.M., Carmichael, I.E., Langmuir, C.H., 1986. Oxidation states of mid-ocean ridge basalt glasses. Earth Planet. Sci. Lett. 79, 397–411.
Chung, S.L., Jahn, B.M., 1995. Plume-lithosphere interaction in generation of the Emeishan flood basalts at the Permian-Triassic boundary. Geology 23, 889–892.
Danyushevsky, L.V., Della-Pasqua, F., Sokolov, S., 2000. Re-equilibration of melt inclusions trapped by magnesian olivine phenocrysts from subduction-related magmas: petrological implications. Contrib. Mineral. Petrol. 138, 68–83.
Danyushevsky, L.V., McNeill, A.W., Sobolev, A.V., 2002. Experimental and petrological studies of melt inclusions in phenocrysts from mantle-derived magmas: an overview of techniques, advantages and complications. Chem. Geol. 183, 5–24.
Ford, C.E., 1981. Parental liquids of the Skaergaard intrusion cumulates. Nature 291, 21–25.
Ford, C.E., Russell, D.G., Craven, J.A., Fisk, M.R., 1983. Olivine-liquid equilibria: temperature, pressure, and composition dependence of the crystal/liquid cation partition coefficient for Mg, Fe^{2+}, Ca and Mn. J. Petrol. 24, 256–266.
Ghiorso, M.S., Sack, R.O., 1995. Chemical mass transfer in magmatic processes. IV. A revised and internally consistent thermodynamic model for the interpolation and extrapolation of liquid-solid equilibria in magmatic systems at elevated temperatures and pressures. Contrib. Mineral. Petrol. 119, 197–212.
Green, H.W., Radcliffe, S.V., 1972. Dislocation mechanisms in olivine and flow in the upper mantle. Earth Planet. Sci. Lett. 15, 239–247.
Greenwood, R.C., Donaldson, C.H., Emeleus, C.H., 1990. The contact zone of the Rhum ultrabasic intrusion: evidence of peridotite formation from magnesian magmas. J. Geol. Soci. 147, 209–212.
Hanski, E., Kamenetsky, V.S., Luo, Z.Y., Xu, Y.G., Kuzmin, D.V., 2010. Primitive magmas in the Emeishan Large Igneous Province, southwestern China and northern Vietnam. Lithos 119, 75–90.
Harmer, R.E., Sharpe, M.R., 1985. Field relations and strontium isotope systematics of the marginal rocks of the eastern Bushveld Complex. Econ. Geol. 80, 813–837.
Hong, L.B., Zhang, Y.H., Qian, S.P., 2013. Constraints from melt inclusions and their host olivines on the petrogenesis of Oligocene-Early Miocene Xindian basalts, Chifeng area, North China Craton. Contrib. Mineral. Petrol. 165, 305–326.
Hoover, J.D., 1989. The chilled marginal gabbro and other contact rocks of the Skaergaard intrusion. J. Petrol. 30, 441–476.
Hou, T., Zhang, Z., Kusky, T., Du, Y., Liu, J., Zhao, Z., 2011. A reappraisal of the high-Ti and low-Ti classification of basalts and petrogenetic linkage between basalts and mafic–ultramafic intrusions in the Emeishan Large Igneous Province, SW China. Ore Geol. Rev. 41, 133–143.
Howarth, G.H., Prevec, S.A., Zhou, M.F., 2013. Timing of Ti-magnetite crystallisation and silicate disequilibrium in the Panzhihua mafic layered intrusion: implications for ore-forming processes. Lithos 170, 73–89.
Jakobsen, J.K., Veksler, I.V., Tegner, C., Brooks, C.K., 2005. Immiscible iron-and silica-rich melts in basalt petrogenesis documented in the Skaergaard intrusion. Geology 33, 885–888.
Jakobsen, J.K., Veksler, I.V., Tegner, C., Brooks, C.K., 2011. Crystallization of the Skaergaard intrusion from an emulsion of immiscible iron-and silica-rich liquids: evidence from melt inclusions in plagioclase. J. Petrol. 52, 345–373.
Kamenetsky, V.S., Chung, S.L., Kamenetsky, M.B., Kuzmin, D.V., 2012. Picrites from the Emeishan Large Igneous Province, SW China: a Compositional Continuum in Primitive Magmas and their Respective Mantle Sources. J. Petrol. 53, 2095–2113.
Kent, A.J.R., 2008. Melt inclusions in basaltic and related volcanic rocks. Rev. Mineral. Geochem. 69, 273–331.
Kruger, F.J., 2005. Filling the Bushveld Complex magma chamber: lateral expansion, roof and floor interaction, magmatic unconformities, and the formation of giant chromitite, PGE and Ti-V-magnetitite deposits. Mineral. Deposita 40, 451–472.
Kuzmin, D.V., Sobolev, A.V., 2004. Boundary layer contribution to the composition of melt inclusions in olivine. Geochim. Cosmochim. Acta. 68, A544.
Le Bas, M.J., Le Maitre, R.W., Streckeisen, A., Zanettin, B., 1986. A chemical classification of volcanic rocks based on the total alkali-silica diagram. J. Petrol. 27, 745–750.
Li, C., Naldrett, A.J., Ripley, E.M., 2007. Controls on the Fo and Ni contents of olivine in sulfide-bearing mafic/ultramafic intrusions: principles, modeling and examples from Voisey's Bay. Earth Sci. Front. 14, 177–185.
Li, C., Xu, Z.H., Waal, S.A., Ripley, E.M., Maier, W.D., 2004. Compositional variations of olivine from the Jinchuan Ni-Cu sulfide deposit, western China: implications for ore genesis. Mineral. Deposita 39, 159–172.
Liu, J.Q., Ren, Z.Y., Nichols, A.R., Song, M.S., Qian, S.P., Zhang, Y., Zhao, P.P., 2015. Petrogenesis of Late Cenozoic basalts from North Hainan Island: constraints from melt inclusions and their host olivines. Geochim. Cosmochim. Acta 152, 89–121.
Liu, P.-P., Zhou, M.-F., Ren, Z., Wang, C.Y., Wang, K., 2016. Immiscible Fe- and Si-rich silicate melts in plagioclase from the Baima mafic intrusion (SW China): implications for the origin of bi-modal igneous suites in large igneous provinces. J. Asian Earth Sci. 127, 211–230.

Mallmann, G., O'Neill, H.C., 2009. The crystal/melt partitioning of V during mantle melting as a function of oxygen fugacity compared with some other elements (Al, P, Ca, Sc, Ti, Cr, Fe, Ga, Y, Zr and Nb). J. Petrol. 50, 1765–1794.
Mathez, E.A., 1984. Influence of degassing on oxidation states of basaltic magmas. Nature 310, 371–375.
Norman, M.D., Garcia, M.O., Kamenetsky, V.S., Nielsen, R.L., 2002. Olivine-hosted melt inclusions in Hawaiian picrites: equilibration, melting, and plume source characteristics. Chem. Geol. 183, 143–168.
Qian, S.P., Ren, Z.Y., Zhang, L., Hong, L.B., Liu, J.Q., 2015. Chemical and Pb isotope composition of olivine-hosted melt inclusions from the Hannuoba basalts, North China Craton: implications for petrogenesis and mantle source. Chem. Geol. 401, 111–125.
Ren, Z.Y., Ingle, S., Takahashi, E., Hirano, N., Hirata, T., 2005. The chemical structure of the Hawaiian mantle plume. Nature 436, 837–840.
Ren, Z.Y., Takahashi, E., Orihashi, Y., Johnson, K.T.M., 2004. Petrogenesis of tholeiitic lavas from the submarine Hana Ridge, Haleakala Volcano, Hawaii. J. Petrol. 45, 2067–2099.
Roeder, P.L., Emslie, R.F., 1970. Olivine-liquid equilibrium. Contrib. Mineral. Petrol. 29, 275–289.
Roedder, E., 1979. Origin and significance of magmatic inclusions. Bull. Mineral. 102, 487–510.
Shellnutt, J.G., Jahn, B.-M., 2011. Origin of Late Permian Emeishan basaltic rocks from the Panxi region (SW China): implications for the Ti-classification and spatial–compositional distribution of the Emeishan flood basalts. J. Volcanol. Geotherm. Res. 199, 85–95.
Sobolev, A.V., 1996. Melt inclusions in minerals as a source of principle petrological information. Petrology 4, 209–220.
Sobolev, A.V., Hofmann, A.W., Kuzmin, D.V., Yaxley, G.M., Arndt, N.T., Chung, S.L., Danyushevsky, L.V., Elliott, T., Frey, F.A., Garcia, M.O., Gurenko, A.A., Kamenetsky, V.S., Kerr, A.C., Krivolutskaya, N.A., Matvienkov, V.V., Nikogosian, I.K., Rocholl, A., Sigurdsson, I.A., Sushchevskaya, N.M., Teklay, M., 2007. The amount of recycled crust in sources of mantle-derived melts. Science 316, 412–417.
Song, X.Y., Zhou, M.F., Keays, R.R., Cao, Z.M., Sun, M., Qi, L., 2006. Geochemistry of the Emeishan flood basalts at Yangliuping, Sichuan, SW China: implication for sulphide segregation. Contrib. Mineral. Petrol. 152, 53–74.
Song, X.Y., Zhou, M.F., Tao, Y., Xiao, J.F., 2008. Controls on the metal compositions of magmatic sulfide deposits in the Emeishan large igneous province, SW China. Chem. Geol. 253, 38–49.
Sours-Page, R., Johnson, K.T.M., Nielsen, R.L., Karsten, J.L., 1999. Local and regional variation of MORB parent magmas: evidence from melt inclusions from the Endeavour Segment of the Juan de Fuca Ridge. Contrib. Mineral. Petrol. 134, 342–363.
Spandler, C., Mavrogenes, J., Arculus, R., 2005. Origin of chromitites in layered intrusions: Evidence from chromite-hosted melt inclusions from the Stillwater Complex. Geology 33, 893–896.
Tao, Y., Hu, R.Z., Qi, L., Luo, T.Y., 2007a. Geochemical characteristics and metallogenesis of the Limahe mafic-ultramafic intrusion, Sichuan. Acta Petrol. Sin. 23, 2785–2800.
Tao, Y., Hu, R.Z., Qi, L., Qu, W.J., Chu, Z.Y., Gou, T.Z., 2010. Sr-Nd-Os isotopic constraints on magma origin and evolution of the Jinbaoshan Pt-Pd deposit, Yunnan. J. Mineral. Petrol. 30, 60–67.
Tao, Y., Li, C., Hu, R.Z., Ripley, E.M., Du, A., Zhong, H., 2007b. Petrogenesis of the Pt-Pd mineralized Jinbaoshan ultramafic intrusion in the Permian Emeishan Large Igneous Province, SW China. Contrib. Mineral. Petrol. 153, 321–337.
Tao, Y., Li, C., Song, X.Y., Ripley, E.M., 2008. Mineralogical, petrological, and geochemical studies of the Limahe mafic-ultramafic intrusion and associated Ni–Cu sulfide ores, SW China. Miner. Depos. 43, 849–972.
Wang, C.Y., Zhou, M.F., Keays, R.R., 2006. Geochemical constraints on the origin of the Permian Baimazhai mafic-ultramafic intrusion, SW China. Contrib. Mineral. Petrol. 152, 309–321.
Wang, C.Y., Zhou, M.F., Qi, L., 2007. Permian flood basalts and mafic intrusions in the Jinping (SW China)-Song Da (northern Vietnam) district: mantle sources, crustal contamination and sulfide segregation. Chem. Geol. 243, 317–343.
Wang, C.Y., Zhou, M.F., Qi, L., 2011. Chalcophile element geochemistry and petrogenesis of high-Ti and low-Ti magmas in the Permian Emeishan large igneous province, SW China. Contrib. Mineral. Petrol. 161, 237–254.
Wang, C.Y., Zhou, M.F., Sun, Y.L., Arndt, N.T., 2012a. Differentiation, crustal contamination and emplacement of magmas in the formation of the Nantianwan mafic intrusion of the ~260 Ma Emeishan large igneous province, SW China. Contrib. Mineral. Petrol. 164, 281–301.
Wang, C.Y., Zhou, M.F., Yang, S.H., Qi, L., Sun, Y.L., 2014. Geochemistry of the Abulangdang intrusion: Cumulates of high-Ti picritic magmas in the Emeishan large igneous province, SW China. Chem. Geol. 378, 24–39.
Wang, C.Y., Zhou, M.F., Zhao, D.G., 2005. Mineral chemistry of chromite from the Permian Jinbaoshan Pt-Pd-sulfide-bearing ultramafic intrusion in SW China with petrogenetic implications. Lithos 83, 47–66.
Wang, D.H., Luo, Y.N., Fu, D.M., Chu, Y.S., 2001. Petrochemistry and ore potentiality of the Mafic-Ultramafic Rocks in the Yangliuping Cu-Ni-PGF Mine, Sichuan Province. Acta Geos. Sin. 22, 135–140 (in Chinese with English abstract).
Wang, M., Zhang, Z.C., Encarnacion, J., Hou, T., Luo, W.J., 2012b. Geochronology and geochemistry of the Nantianwan mafic-ultramafic complex, Emeishan large igneous province: metallogenesis of magmatic Ni-Cu sulphide deposits and geodynamic setting. Int. Geol. Rev. 54, 1746–1764.
Wang, Z.R., Gaetani, G.A., 2008. Partitioning of Ni between olivine and siliceous eclogite partial melt: experimental constraints on the mantle source of Hawaiian basalts. Contrib. Mineral. Petrol. 156, 661–678.
Weis, D., Kieffer, B., Maerschalk, C., 2005. High – precision Pb-Sr-Nd-Hf isotopic characterization of USGS BHVO-1 and BHVO-2 reference materials. Geochem. Geophys. Geosyst. http://dx.doi.org/10.1029/2004GC000852.
Xiao, L., Xu, Y.G., Mei, H.J., Zheng, Y.F., He, B., Pirajno, F., 2004. Distinct mantle sources of low-Ti and high-Ti basalts from the western Emeishan large igneous province, SW China: implications for plume-lithosphere interaction. Earth Planet. Sci. let. 228, 525–546.
Xu, J.F., Suzuki, K., Xu, Y.G., Mei, H.J., Li, J., 2007. Os, Pb, and Nd isotope geochemistry of the Permian Emeishan continental flood basalts: insights into the source of a large igneous province. Geochim. Cosmochim. Acta 70, 2104–2119.
Xu, Y.G., Chung, S.L., Jahn, B.M., Wu, G.Y., 2001. Petrologic and geochemical constraints on the petrogenesis of Permian-Triassic Emeishan flood basalts in southwestern China. Lithos 58, 145–168.
Xu, Y.G., Wang, C.Y., Shen, S., 2014. Permian large igneous provinces: characteristics, mineralization and paleo-environment effects. Lithos 204, 1–3.
Zhang, H.F., Gao, S., Zhang, B.R., Luo, T.C., Lin, W.L., 1997. Pb isotopes of granitoids suggest Devonian accretion of Yangtze (South China) craton to North China craton. Geology 25, 1015–1018.
Zhang, L., Ren, Z.Y., Nichols, A.R., Zhang, Y.H., Zhang, Y., Qian, S.P., Liu, J.Q., 2014. Lead isotope analysis of melt inclusions by LA-MC-ICP-MS. J. Anal. At. Spectrom. 29, 1393–1405.
Zhang, Y., Ren, Z.Y., Xu, Y.G., 2013. Sulfur in olivine-hosted melt inclusions from the Emeishan picrites: implications for S degassing and its impact on environment. J. Geophys. Res. 118, 4063–4070.
Zhang, Z.C., Mahoney, J.J., Mao, J.W., Wang, F.H., 2006. Geochemistry of picritic and associated basalt flows of the western Emeishan flood basalt province, China. J. Petrol. 47, 1997–2019.
Zhou, M.-F., Malpas, J., Song, X., Kennedy, A.K., Robinson, P.T., Sun, M., Lesher, C.M., Keays, R.R., 2002. A temporal link between the Emeishan large igneous province (SW China) and the end-Guadalupian mass extinction. Earth Planet. Sci. let. 196, 113–122.
Zhou, M.-F., Arndt, N.T., Malpas, J., Wang, C.Y., Kennedy, A.K., 2008. Two magma series and associated ore deposit types in the Permian Emeishan large igneous province, SW China. Lithos 103, 352–368.
Zhu, F.L., Tao, Y., Hu, R.Z., Yu, S.Y., Qu, W.J., Du, A.D., 2011. Re-Os isotopic constraints on the ore-forming mechanism for the Qingkuangshan Ni-Cu-PGE deposit in the Huili County, Sichuan Province. Acta Petrol. Sin. 27, 2655–2664 (in Chinese with English abstract).